Overview and Evaluation of Energy Balancing Techniques for MMCs with Various Input and Output Frequencies

Gyanendra Kumar Sah, Michael Schütt, Hans-Günter Eckel

UNIVERSITY OF ROSTOCK
Albert-Einstein-Str.2
D-18059 Rostock, Germany
Tel.: +49 / (0) 381 – 498 7137.
Fax: +49 / (0) 381 – 498 7102.
E-Mail: gyanendra.sah@uni-rostock.de
URL: http://www.iee.uni-rostock.de

Acknowledgments

This paper was made within the framework of the research project *Netz-Stabil* and financed by the European Social Fund (ESF/14-BM-A55-0015/16). This paper is part of the qualification program *Promotion of Young Scientists in Excellent Research Associations - Excellence Research Programme of the State of Mecklenburg-Western Pomerania*.

Keywords

«Modular Multilevel Converters (MMC)», «Capacitor Voltage Balancing», «AC-AC Converter», «Grid-Connected Converter», «Energy Balancing»

Abstract

This work provides an overview of all possible arm energy regulation techniques for the *Modular Multilevel Converter* (MMC). This research aims to identify all degrees of freedom (manipulated inputs) and possible combinations to regulate the arm energies of the MMC. Further, it offers a new generalized analytical toolchain to compare and evaluate the stability and performance of these balancing techniques. This toolchain includes normal operation, failure operation, and different three-phase and single-phase frequency conditions such as equal and unequal frequency applications (AC/AC, DC/AC). The common-mode voltage plays an essential role in regulating arm energies of the MMC for equal frequency operation. The proposed toolchain can also help to validate dimensioning of the converter analytically. Any existing energy balancing technique for MMC could be linked directly or indirectly to all derived energy balancing methods.

Introduction

The MMC is a promising topology for high-power applications, especially in the medium-voltage range [1, 2]. The MMC provides various degrees of freedom (manipulated inputs) to regulate its arm energies. Hence, multiple methods can be derived using a combination of these manipulated inputs to control the arm energies of the MMC. Some arm energy regulation techniques may not work for equal and unequal single-phase and three-phase frequency operations, which will be discussed later. Therefore, stability and performance analysis of the arm energy regulation techniques, especially for all expected (normal and abnormal) operating conditions, should be investigated before actual hardware implementation. It would further help if this investigation could be performed analytically, saving time, staffing, and money.

The common-mode voltage introduces an additional degree of freedom to regulate the arm energies of MMC [3]. The main objective of this work is to present a detailed mathematical toolchain for the investigation of various possible degrees of freedom to regulate arm energies of the MMC for different

single-phase and three-phase frequency conditions. Further, the proposed toolchain facilitates analytical validation of the dimensioning of the converter during normal and abnormal operating conditions.

MMC Topology and Transformed Arm Powers in the αβ0-Frame

An accurate average electrical circuit diagram plays a vital role in deriving governing plant equations, which are later used for designing a suitable controller. Fig. 1.a illustrates the average equivalent electrical circuit diagram of direct MMC topology [1]. Here, v_{a123}, $v_{b,}$ and v_{cm} represent three-phase, single-phase, and common-mode voltages. v_{cm} can be either DC or AC. The frequency of AC v_{cm} (f_{cm}) is generally chosen differently than the single-phase (f_b) and three-phase (f_a) frequencies, the proposed relation is $f_{cm} = 3\text{Max}(f_a, f_b)$. The neutral point (N) of the three-phase voltage source can be either floating or grounded. Each controlled arm voltage source ($v_{p/ny}$) represents a mathematical model of various submodules (SMs) connected in series. Depending upon the single-phase and three-phase frequencies, an SM is realized using either a full-bridge or half-bridge converter. Full-bridge-based SMs can be used universally, whereas half-bridge-based SMs cannot be used for equal frequency operation. Each branch current ($i_{p/ny}$) can be decomposed into two components: (a) circulating current (i_{by}) and (b) three-phase current ($0.5i_{ay}$). The expression of the summation and difference arm currents ($i_{\Sigma/\Delta y}$) and arm voltages ($v_{\Sigma/\Delta y}$) for phase y of MMC are shown in Fig. 1. The circulating current is the same for both the upper and lower arms in a phase. Fig. 1b represents the MMC topology and visualizes the energy components of the structure after ignoring all arm impedances (Z_{arm}). (1) illustrates the summation and difference arm powers of phase y of MMC. (2) to (7) represent the expression for the instantaneous summation and difference arm powers in the αβ0-frame [3, 4].

$$p_{\Sigma y} = p_{py} + p_{ny} \;;\; p_{\Delta y} = p_{py} - p_{ny} \tag{1}$$

$$p_{\Sigma\alpha} = v_b\, i_{b\alpha} + v_{cm}\, i_{a\alpha} + \frac{v_{a\alpha}\, i_{a\alpha} - v_{a\beta}\, i_{a\beta}}{2} \tag{2}$$

$$p_{\Sigma\beta} = v_b\, i_{b\beta} + v_{cm}\, i_{a\beta} - \frac{v_{a\alpha}\, i_{a\beta} + v_{a\beta}\, i_{a\alpha}}{2} \tag{3}$$

$$p_{\Sigma 0} = v_b\, i_{b0} + \frac{v_{a\alpha}\, i_{a\alpha} + v_{a\beta}\, i_{a\beta}}{2} \tag{4}$$

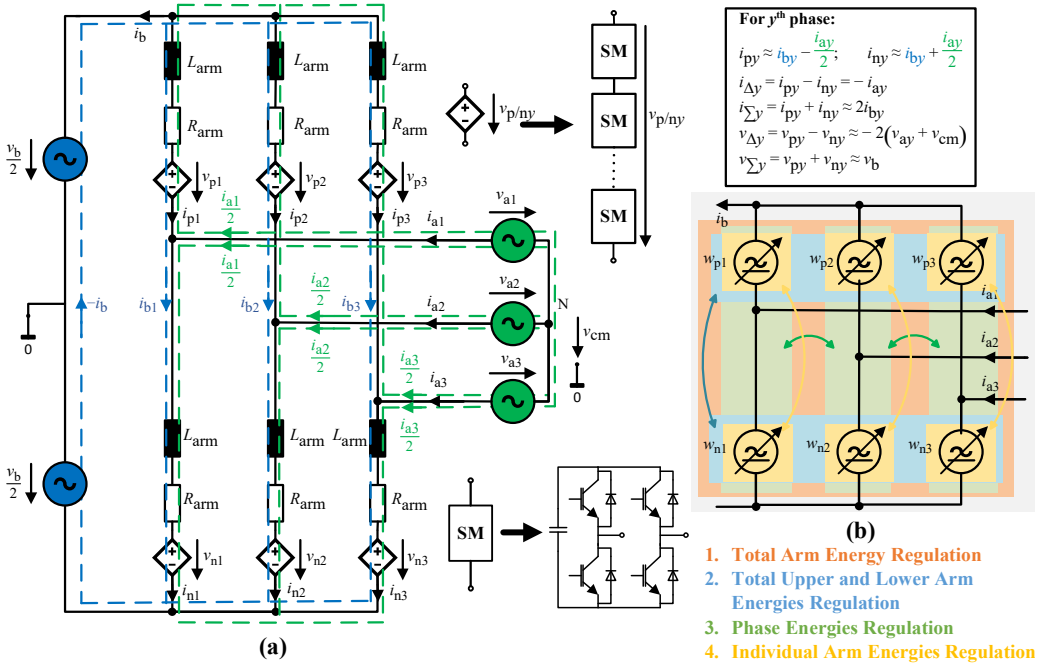

Fig. 1: Average equivalent electrical circuit diagram and arm energy regulations of MMC.

Table I: Different *Manipulated Inputs* (MIs) for regulating corresponding average arm energies of MMC.

1. Total Arm Energy Regulation (MI_1)	**2. Total Upper and Lower Arms Energies Regulation (MI_2)**
Positive sequence three-phase currents in the d-axis $\left(i_{\mathrm{ad+}}\right)$.	Positive sequence circulating currents in the d-axis $\left(i_{\mathrm{bd+}}\right)$.
Zero sequence circulating current in phase with $v_{\mathrm{b}}\left(i_{\mathrm{b0}}^{\mathrm{b}}\right)$.	Zero sequence circulating current in phase with $v_{\mathrm{cm}}\left(i_{\mathrm{b0}}^{\mathrm{cm}}\right)$.
3. Phase Energies Regulation (MI_{34})	**4. Individual Arm Energies Regulation (MI_{56})**
Circulating currents in phase with $v_{\mathrm{b}}\left(i_{\mathrm{b}\alpha\beta}^{\mathrm{b}}\right)$.	Three-phase currents in phase with $v_{\mathrm{b}}\left(i_{\mathrm{a}\alpha\beta}^{\mathrm{b}}\right)$.
Three-phase currents in phase with $v_{\mathrm{cm}}\left(i_{\mathrm{a}\alpha\beta}^{\mathrm{cm}}\right)$.	Single-phase currents in phase with $v_{\mathrm{a}\alpha\beta}$ $\left(i_{\mathrm{b0}}^{\mathrm{a\text{-}}\alpha\beta}\right)$.
Negative sequence three-phase currents $\left(i_{\mathrm{adq}-}\right)$.	Circulating currents in phase with $v_{\mathrm{cm}}\left(i_{\mathrm{b}\alpha\beta}^{\mathrm{cm}}\right)$.
Note: $i_{\mathrm{b0}} = -\frac{i_{\mathrm{b}}}{3}$	Negative sequence circulating currents $\left(i_{\mathrm{bdq}-}\right)$.

$$p_{\Delta\alpha} = -\frac{v_{\mathrm{b}}\, i_{\mathrm{a}\alpha}}{2} - 2v_{\mathrm{a}\alpha}\, i_{\mathrm{b0}} - 2v_{\mathrm{cm}}\, i_{\mathrm{b}\alpha} - v_{\mathrm{a}\alpha}\, i_{\mathrm{b}\alpha} + v_{\mathrm{a}\beta}\, i_{\mathrm{b}\beta} \tag{5}$$

$$p_{\Delta\beta} = -\frac{v_{\mathrm{b}}\, i_{\mathrm{a}\beta}}{2} - 2v_{\mathrm{a}\beta}\, i_{\mathrm{b0}} - 2v_{\mathrm{cm}}\, i_{\mathrm{b}\beta} + v_{\mathrm{a}\alpha}\, i_{\mathrm{b}\beta} + v_{\mathrm{a}\beta}\, i_{\mathrm{b}\alpha} \tag{6}$$

$$p_{\Delta 0} = -2v_{\mathrm{cm}}\, i_{\mathrm{b0}} - v_{\mathrm{a}\alpha}\, i_{\mathrm{b}\alpha} - v_{\mathrm{a}\beta}\, i_{\mathrm{b}\beta} \tag{7}$$

All Possible Manipulated Inputs for Regulation of Arm Energies of MMC

Knowing all degrees of freedom can help derive all possible arm energy regulation techniques for the MMC. The arm energies ($W_{\Sigma/\Delta\alpha\beta0}$) of the MMC can be regulated by varying the corresponding arm powers ($p_{\Sigma/\Delta\alpha\beta0}$), which can be achieved by changing the *Manipulated Inputs* (MIs): circulating currents ($i_{\mathrm{b}\alpha\beta}$) and three-phase currents ($i_{\mathrm{a}\alpha\beta}$) (or single-phase current (i_{b0})).

The equations (2) and (3) represent the influence on the phase energies (MI_{34}) – see Fig.1(b). Similarly, equation (4) shows the influence on the total arm energy (MI_1), (5) and (6) the individual arm energies (MI_{56}), and (7) the total upper and lower arm energies (MI_2).

(8) represents the currents in the αβ-frame only due to the positive and negative sequence currents in the dq-frame. The Park and inverse Park transformation angle (θ_{a}) can be obtained from the output of the three-phase voltage *Phase-Locked Loop* (PLL). Since the same frequency components of current and voltage components make power, negative sequence currents also produce average power and thus represent one of the manipulated inputs according to (2) – (6), and (10). Table I lists all possible manipulated inputs for regulating corresponding arm energies (see also (2) to (10), and Fig. 1b). i_x^y represents current component (manipulated input) i_x in phase with the voltage v_y.

Table. II: Stability analysis of various average arm energies regulation techniques for direct AC-AC and AC-DC MMC topologies. Here, n = odd integers and $f_{cm} = 3\text{Max}(f_a, f_b)$.

Method	Manipulated Inputs (MI_1,MI_2,MI_{34}, MI_{56})	Determinant (|A|)	
		$f_a = f_b$	$f_a = n\,f_b, f_b = n\,f_a$ & f_b = DC
1	i_{ad+}, i_{bd+}, $i^{b}_{b\alpha\beta}$, i_{bdq-}	0	$2\,V_a^4\,V_b^2$
2	i_{ad+}, i_{bd+}, $i^{b}_{b\alpha\beta}$, $i^{b}_{a\alpha\beta}$	$\frac{V_a^2}{16}\left(\cos^2(3\phi_b)\,V_a^2\,V_b^2 - \left(2V_a^2 - V_b^2\right)^2\right)$	$-\frac{1}{4}\,V_a^2\,V_b^4$
3	i_{ad+}, i_{bd+}, i_{adq-}, i_{bdq-}	$-\,V_a^2\left(V_a^2 - \frac{V_b^2}{4}\right)^2$	$-\,V_a^6$
4	i_{ad+}, i_{bd+}, i_{adq-}, $i^{b}_{a\alpha\beta}$	0	$\frac{1}{8}\,V_a^4\,V_b^2$
5	i^{b}_{b0}, i_{bd+}, $i^{b}_{b\alpha\beta}$, i_{bdq-}	0	$2\sqrt{2}\,V_a^3\,V_b^3$
6	i^{b}_{b0}, i_{bd+}, $i^{b}_{b\alpha\beta}$, $i^{a\text{-}\alpha\beta}_{b0}$	0	$-\,4\sqrt{2}\,V_a^3\,V_b^3$
7	i_{ad+}, i_{bd+}, $i^{b}_{b\alpha\beta}$, $i^{cm}_{b\alpha\beta}$	$-\,2\,V_a^2\,V_b^2\,V_{cm}^2$	$-\,4\,V_a^2\,V_b^2\,V_{cm}^2$
8	i_{ad+}, i_{bd+}, $i^{cm}_{a\alpha\beta}$, $i^{b}_{a\alpha\beta}$	$-\frac{1}{8}\,V_a^2\,V_b^2\,V_{cm}^2$	$-\frac{1}{4}\,V_a^2\,V_b^2\,V_{cm}^2$
9	i_{ad+}, i_{bd+}, $i^{cm}_{a\alpha\beta}$, $i^{cm}_{b\alpha\beta}$	$-\,4\,V_a^2\,V_{cm}^4$	$-\,4\,V_a^2\,V_{cm}^4$
10	i_{ad+}, i_{bd+}, $i^{cm}_{a\alpha\beta}$, i_{bdq-}	$2\,V_a^4\,V_{cm}^2$	$2\,V_a^4\,V_{cm}^2$
11	i_{ad+}, i_{bd+}, i_{adq-}, $i^{cm}_{b\alpha\beta}$	$2\,V_a^4\,V_{cm}^2$	$2\,V_a^4\,V_{cm}^2$
12	i^{b}_{b0}, i_{bd+}, $i^{b}_{b\alpha\beta}$, $i^{cm}_{b\alpha\beta}$	$-\,2\sqrt{2}\,V_a\,V_b^3\,V_{cm}^2$	$-\,4\sqrt{2}\,V_a\,V_b^3\,V_{cm}^2$
13	i^{b}_{b0}, i^{cm}_{b0}, $i^{b}_{b\alpha\beta}$, $i^{a\text{-}\alpha\beta}_{b0}$	0	$-\,8\,V_a^2\,V_b^3\,V_{cm}$
14	i^{b}_{b0}, i^{cm}_{b0}, $i^{b}_{b\alpha\beta}$, $i^{cm}_{b\alpha\beta}$	$-\,8\,V_b^3\,V_{cm}^3$	$-\,8\,V_b^3\,V_{cm}^3$
15	i^{b}_{b0}, i^{cm}_{b0}, $i^{b}_{b\alpha\beta}$, i_{bdq-}	$V_a^2\,V_b^3\,V_{cm}$	$4V_a^2\,V_b^3\,V_{cm}$

In summary, the components of the circulating current ($i_{b\alpha\beta}$), the three-phase current ($i_{a\alpha\beta}$), and the single-phase current ($i_b = -\,i_{b0}/3$)) which are in phase with the single-phase voltage (v_b), three-phase voltage ($v_{a\alpha\beta}$), and common-mode voltage (v_{cm}) represent the manipulated inputs of the power equations. Any combination of the six manipulated inputs (MI_1, MI_2, MI_{34}, MI_{56}) from Table. I represent a possible energy balancing technique for the MMC. Any existing energy balancing technique for MMC could be linked directly or indirectly to all derived energy balancing methods from Table. I.

$$i_{\alpha\beta} = D(\theta_a)\, i_{dq+} + \overset{-1}{D(\theta_a)}\, i_{dq-} \rightarrow \begin{pmatrix} i_\alpha \\ i_\beta \end{pmatrix} = \begin{pmatrix} \cos(\theta_a)\left(i_{d+} + i_{d-}\right) + \sin(\theta_a)\left(i_{q-} - i_{q+}\right) \\ \cos(\theta_a)\left(i_{q+} + i_{q-}\right) + \sin(\theta_a)\left(i_{d+} - i_{d-}\right) \end{pmatrix} \tag{8}$$

$$D(\theta_a) = \begin{pmatrix} \cos(\theta_a) & -\sin(\theta_a) \\ \sin(\theta_a) & \cos(\theta_a) \end{pmatrix} \; ; \; \overset{-1}{D(\theta_a)} = \begin{pmatrix} \cos(\theta_a) & \sin(\theta_a) \\ -\sin(\theta_a) & \cos(\theta_a) \end{pmatrix} \tag{9}$$

$$\overline{\left\{ v_{a\alpha}\, i_{x\alpha} - v_{a\beta}\, i_{x\beta} \right\}} = \hat{V}_{a+}\, i_{xd-} \; ; \; \overline{\left\{ v_{a\alpha}\, i_{x\beta} + v_{a\beta}\, i_{x\alpha} \right\}} = \hat{V}_{a+}\, i_{xq-} \; ; \; \overline{\left\{ v_{a\alpha}\, i_{x\alpha} + v_{a\beta}\, i_{x\beta} \right\}} = \hat{V}_{a+}\, i_{xd+} \tag{10}$$

Average Arm Energies Regulation Techniques for Direct MMC Topology

According to Table I, various energy balancing methods for the MMC can be derived by the combination of the manipulated inputs (MI_1, MI_2, MI_{34}, MI_{56}). (11) illustrates the definition of the three-phase voltage angle (θ_a), single-phase voltage angle (θ_b), and common-mode voltage angle (θ_a). Further, (12) represents the three-phase voltage ($v_{a\alpha\beta}$), single-phase voltage (v_b) and common-mode voltage (v_{cm}) expressions. (13) – (17) show the full expressions of the currents, including the previously mentioned definitions.

These expressions decompose the three-phase currents ($i_{a\alpha\beta}$), the circulating currents ($i_{b\alpha\beta}$), and the single-phase currents ($i_b \approx i_{b0}$) into components that are in phase with the voltages $v_{a\alpha\beta}$, v_b, and v_{cm}. i_{b0}^{-1} and i_{aq+} are used to realize reactive powers in single-phase and three-phase networks, respectively.

These equations change slightly for AC-DC MMC topology. The DC value of the voltages and currents for AC-DC MMC application is equal to the corresponding RMS voltage and RMS currents during

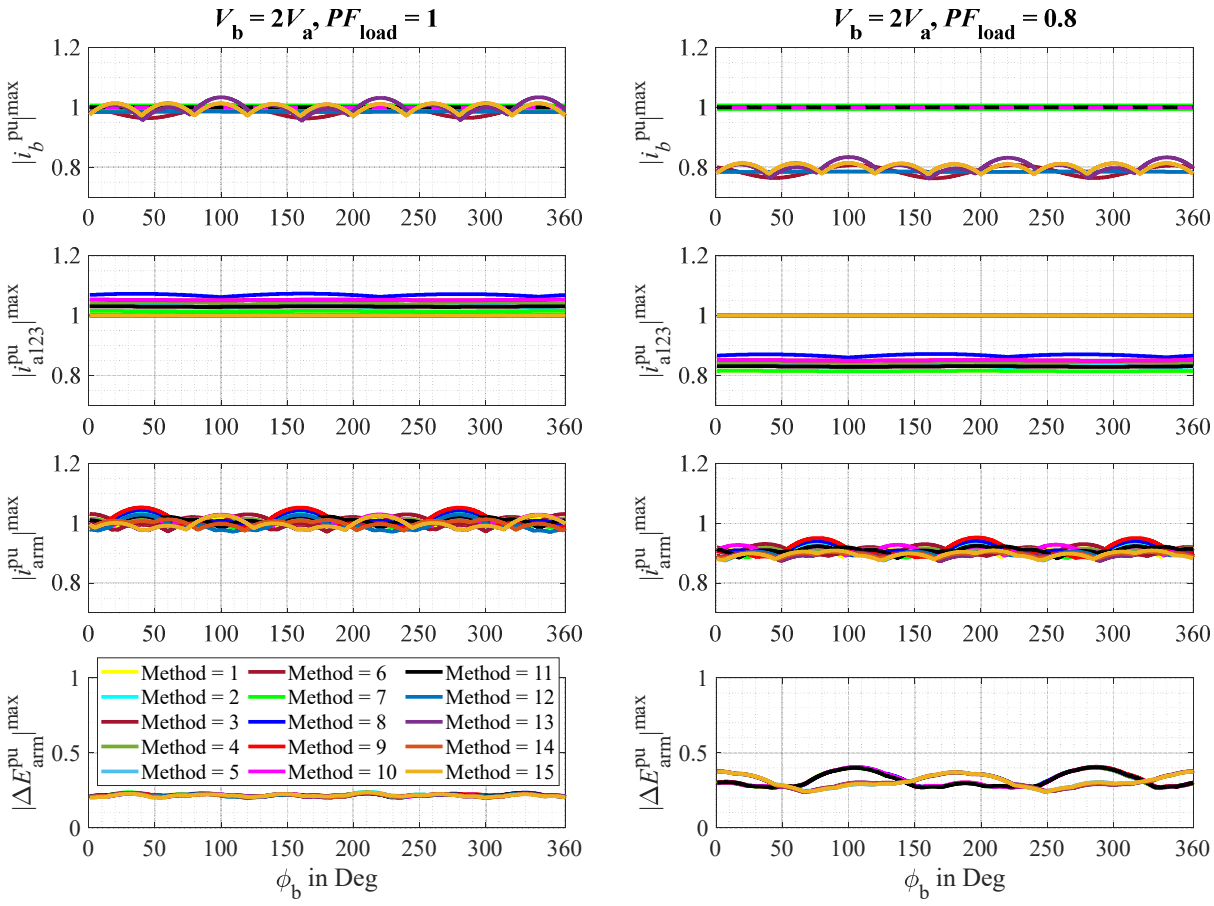

Fig. 2: Performance analysis of direct AC-AC MMC via current and energy values for all stable arm energy regulation techniques for $f_b = f_a/3$ application during normal operations at various load power factor. Here, $V_{cm} = 0.55\ V_a$.

AC-AC MMC application. If the single-phase side provides power, the three-phase currents are used to regulate the overall arm energies, and when the three-phase side acts as a power source, the single-phase currents are used to regulate the arm energies. All possible methods to regulate arm energies using six manipulated inputs (MI_1, MI_2, MI_{34}, MI_{56}) are listed in Table II. Method 1 to 6 represent the energy balancing methods that do not require common-mode voltage. The common-mode frequency (f_{cm}) equals 3Max(f_a, f_b) to avoid couplings with the single-phase and the three-phase networks. It should be noted that harmonics are injected into the grid of the MMC for eleven of the shown energy balancing techniques (Method 2, 3, 4, 6, 8, 9, 10, 11, 13, 14, and 15). No harmonics flow into the grid for four energy balancing methods (Method 1, 5, 7, and 12). One may choose any suitable energy balancing method based on the desired system requirements and controller's performance.

$$\theta_a = \omega_a t\,;\, \theta_b = \omega_b t + \phi_b\,;\, \theta_{cm} = \omega_{cm} t + \phi_{cm} \tag{11}$$

$$v_{a\alpha} = \sqrt{2} V_a \cos(\theta_a),\; v_{a\beta} = \sqrt{2} V_a \sin(\theta_a),\; v_{cm} = \sqrt{2} V_{cm} \cos(\theta_{cm}),\text{ and } v_b = \sqrt{2} V_b \cos(\theta_b) \tag{12}$$

$$i_{a\alpha} = \cos(\theta_a)(i_{ad+} + i_{ad-}) + \sin(\theta_a)(i_{aq-} - i_{aq+}) + \sqrt{2} I_{a\alpha}^{cm} \cos(\theta_{cm}) + \sqrt{2} I_{a\alpha}^{b} \cos(\theta_b) \tag{13}$$

$$i_{a\beta} = \cos(\theta_a)(i_{aq+} + i_{aq-}) + \sin(\theta_a)(i_{ad+} - i_{ad-}) + \sqrt{2} I_{a\beta}^{cm} \cos(\theta_{cm}) + \sqrt{2}\, I_{a\beta}^{b} \cos(\theta_b) \tag{14}$$

$$i_{b\alpha} = \cos(\theta_a)(i_{bd+} + i_{bd-}) + \sin(\theta_a)\, i_{bq-} + \sqrt{2} I_{b\alpha}^{cm} \cos(\theta_{cm}) + \sqrt{2} I_{b\alpha}^{b} \cos(\theta_b) \tag{15}$$

$$i_{b\beta} = \cos(\theta_a) i_{bq-} + \sin(\theta_a)(i_{bd+} - i_{bd-}) + \sqrt{2} I_{b\beta}^{cm} \cos(\theta_{cm}) + \sqrt{2}\, I_{b\beta}^{b} \cos(\theta_b) \tag{16}$$

$$i_{b0} = \sqrt{2} I_{b0}^{\perp b} \sin(\theta_b) + \sqrt{2} I_{b0}^{b} \cos(\theta_b) + \sqrt{2} I_{b0}^{cm} \cos(\theta_{cm}) + \sqrt{2} I_{b0}^{a\text{-}\alpha} \cos(\theta_a) + \sqrt{2} I_{b0}^{a\text{-}\beta} \sin(\theta_a) \tag{17}$$

Stability and Performance Analysis

Validation of controller stability and performance analysis is vital while designing any controller. Arm currents, arm energies, and source current magnitude could be used to examine the performance of the MMC for the selected energy regulation method. For a chosen energy regulation method (see Table II), (18) represents the average of the equations (2) to (7) using matrix notation. Here, P_{6x1} represents the

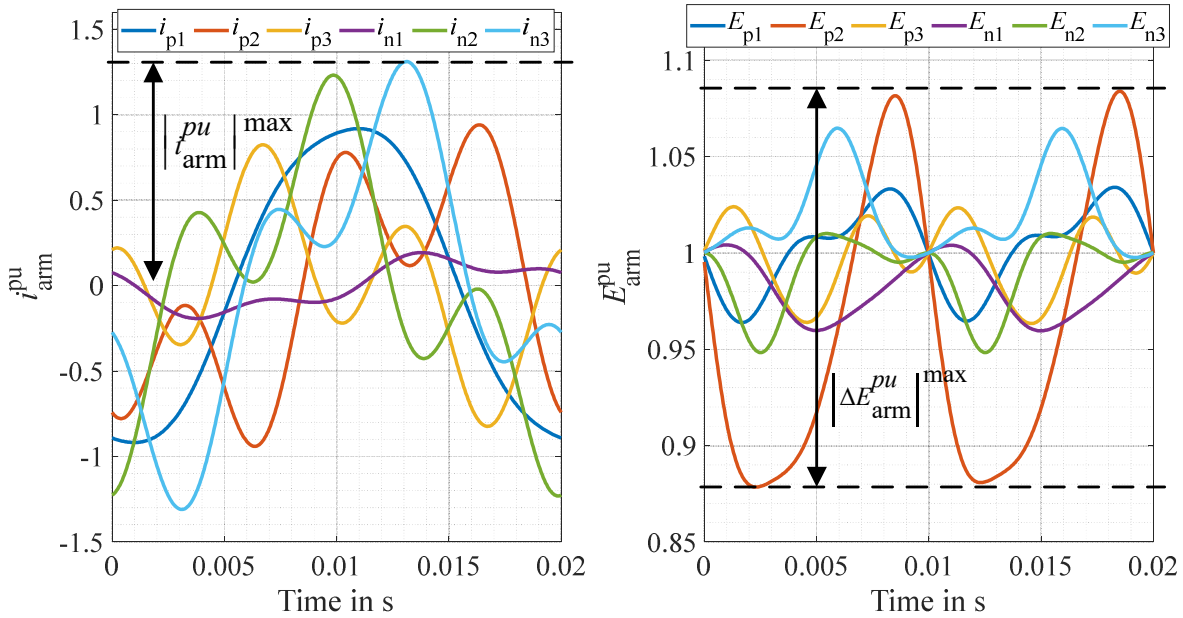

Fig. 3: Definition of *Maximum Arm Current* (left image) and *Arm Energy Ripple* (right image) using an example test case ($f_b = f_a$).

residual power matrix which consists of reactive power and coupling power components. In the steady-state, the average arm energies are constant; hence $\overline{p_{\Sigma/\Delta\alpha\beta0}} = 0$. The frequency for computing average power ($\overline{p_{\Sigma/\Delta\alpha\beta0}}$.) is selected using $f_{avg} = \text{Max}(0, \text{Min}(f_a, f_b))$. (19) represents the solution of (18) with $\overline{p_{\Sigma/\Delta\alpha\beta0}} = 0$. The determinant of the matrix A (|A|) for various methods and operating conditions are also listed in Table II. V_b represents the DC magnitude and RMS magnitude of the single-phase voltage for the AC-DC MMC topology and direct AC-AC MMC topology, respectively. If |A| = 0, the method is unstable. For unequal frequency operations ($f_a = n f_b, f_b = n f_a$ & f_b = DC), where n = odd integers, all methods are stable, and the manipulated inputs are naturally decoupled (A = diagonal matrix).

In contrast, methods 1, 4, 5, 6, and 13 are unstable for equal frequency operation ($f_a = f_b$). Further, Method 2 is unstable at $V_b = 2V_a$, and Method 3 is unstable at $V_b = 2V_a$ and $\phi_b = .m\pi/6$, where m = 0 & even integers for $f_a = f_b$. Hence, all methods without manipulated inputs in phase with v_{cm} (Method 1 to 6) are unstable at $V_b = 2V_a$ and $f_a = f_b$ because of the coupling between the manipulated inputs. These findings suggest that the common-mode voltage plays a vital role in balancing arm energies of direct AC-AC MMC for equal frequency operation.

$$\left(\overline{P_{\Sigma/\Delta\alpha\beta0}}\right)_{6x1} = A_{6x6}\, MI_{6x1} + P_{6x1} \tag{18}$$

$$MI_{6x1} = -A^{-1}_{6x6}\, P_{6x1} \tag{19}$$

Solving (19) gives either RMS or amplitude of the selected manipulated input currents, which are substituted in (13) to (17) to obtain the instantaneous three-phase ($i_{a\alpha\beta}$), circulating ($i_{b\alpha\beta}$) and single-

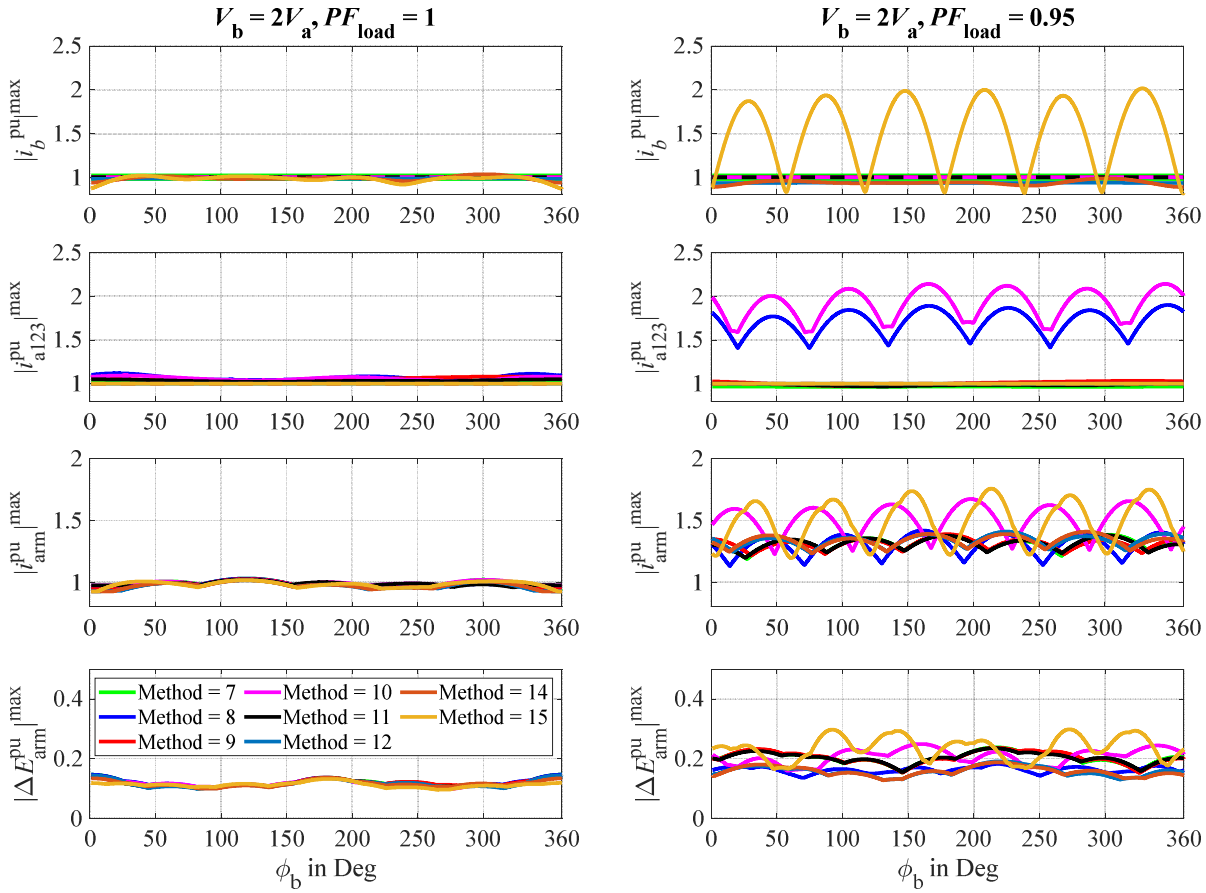

Fig. 4: Performance analysis of direct AC-AC MMC via current and energy values for all stable arm energy regulation techniques for $f_b = f_a$ application during normal operations at various load power factor. Here, $V_{cm} = 0.55\ V_a$.

phase ($i_b \approx i_{b0}$) currents. It should be noted that each energy balancing method uses only six manipulated inputs. Hence, all remaining manipulated input's magnitude is considered zero while computing instantaneous currents using (13) to (17). The three-phase (i_{a123}) and circulating (i_{b123}) currents in the abc-frame are obtained by performing inverse Clarke transformation on $i_{a\alpha\beta}$, and $i_{b\alpha\beta0}$, respectively. The instantaneous arm currents ($i_{p/n123}$) are obtained from i_{a123} and i_{b123} (see Fig. 1). Further, $i_{a\alpha\beta}$, $i_{b0,}$ and $i_{b\alpha\beta}$ are substituted in (2) to (7) to get instantaneous summation and difference arm powers ($p_{\Sigma/\Delta\alpha\beta0}$) in the αβ0-frame, which are transformed to the abc frame using inverse Clarke transformation.

The instantaneous arm powers ($p_{p/n123}$) can be obtained by solving (1). Assuming each arm's energies were initially at the reference value, the instantaneous arm energies ($E_{p/n123}$) are obtained by integrating computed instantaneous arm powers ($p_{p/n123}$).

The ripple in the arm energies ($\Delta E_{p/n123}$) can be computed from the computed instantaneous arm energies. If the maximum arm currents and energies are within the safe limits, then it can be said that the MMC is operating safely. Therefore, the maximum arm currents and arm energies could be investigated to validate the dimensioning of the converter for all operating conditions.

Analytical Result

Fig. 2 shows the solution of the equations for all stable methods at $V_b = 2V_a$ and various load power factors (PF_{load}) for $f_a = 3\,f_b$ operation. The definition of maximum arm currents ($|i_{arm}^{pu}|^{max}$) and maximum ripple arm energy ($|\Delta E_{arm}^{pu}|^{max}$) is illustrated in Fig. 3. The nominal load current with the power factor (PF_{load}) is supplied for all the investigated cases, and no reactive power is drawn from the source of the MMC. The results show that the maximum arm current ($|i_{arm}^{pu}|^{max}$) is reduced when PF_{load} is reduced for $f_a = 3\,f_b$ operation, and the maximum ripple arm energy $|\Delta E_{arm}^{pu}|^{max}$ increases when PF_{load} is reduced. The single-phase reactive power cannot be compensated by the three-phase reactive power and vice versa.

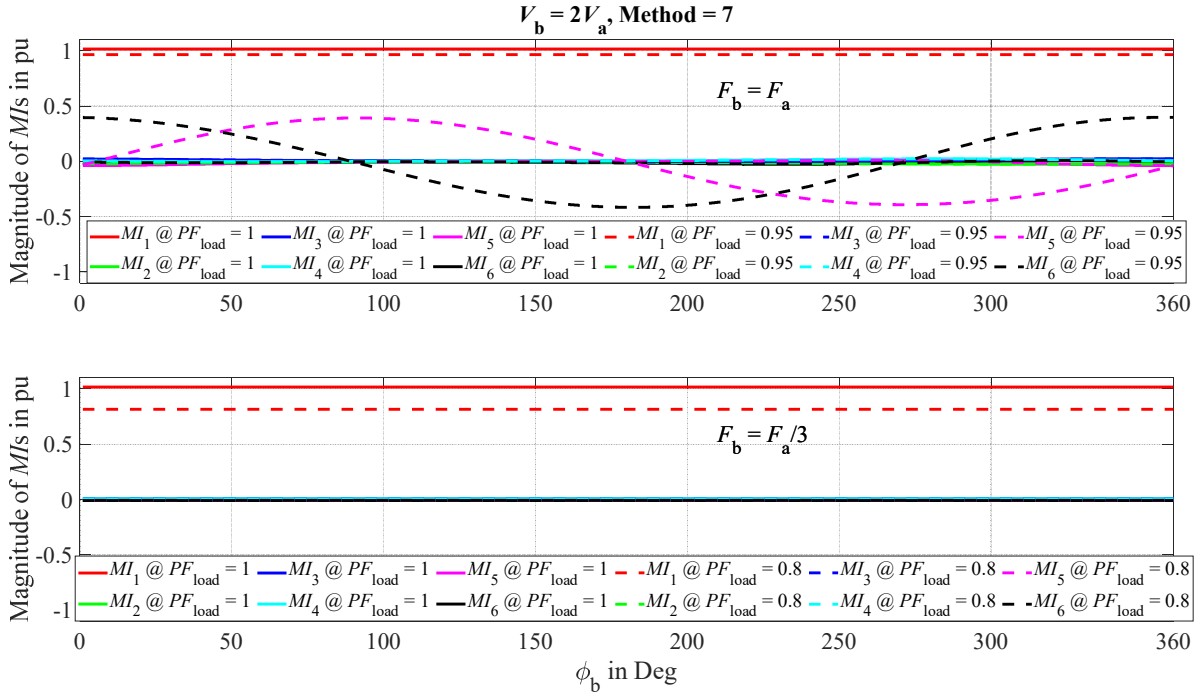

Fig. 5: *Manipulated Inputs* (MI) variation due to *Power Factor* (PF_{load}) change for energy regulation technique using Method-7 ($f_b = f_a/3$ and $f_b = f_a$) during normal operations. Solid line: $PF_{load} = 1$ and dotted line: less PF_{load}

Hence increase in $|\Delta E_{arm}^{pu}|^{max}$ with reduction in PF_{Load} is because the load reactive power oscillates inside MMC, which increases oscillation of the arm energies.

Similarly, Fig. 4 represents the solution of the equations for all stable methods at $V_b = 2V_a$ and various load power factors (PF_{load}) for $f_a = f_b$ operation. Method 8, 10, and 15 are stable, but their performance for $f_b = f_a$ operation is poor compared to other stable methods. In contrast with $f_a = 3\,f_b$ operation, $|i_{arm}^{pu}|^{max}$ increases with a lower power factor at $f_a = f_b$ operation.

The first two terms ($-0.5\,v_b\,i_{a\alpha\beta} - 2\,v_{a\alpha\beta}\,i_{b0}$) on the right-hand side of (5) and (6) represent coupling between the single-phase and three-phase systems. The *Manipulated Inputs* (MIs) only need to compensate for the losses at $f_a = 3\,f_b$ because the three-phase and single-phase systems are naturally decoupled: the third harmonic component does not make power with the fundamental component. For $f_a = f_b$ operation, however, the MIs also compensate for couplings ($-0.5\,v_b\,i_{a\alpha\beta} - 2\,v_{a\alpha\beta}\,i_{b0}$) present in the system. Fig. 5 shows the magnitude of manipulated inputs for both $f_b = f_a$ and $f_b = f_a/3$ operations at unity power factor and low power factor. For equal frequency operation, the coupling is predominant, and its effect also increases with a reduction in power factor. On the other hand, the magnitude of manipulated inputs does not increase with a low power factor for $f_b = f_a/3$ operation.

Fig. 6 represents the analytical results during the failure conditions on the single-phase side for well-behaved stable methods at $f_a = f_b$, and $V_b = 2V_a$. More arm current and more ripple arm energy are observed when the fault location is far away from the MMC because the load power factor is poor, increasing the coupling between manipulated inputs.

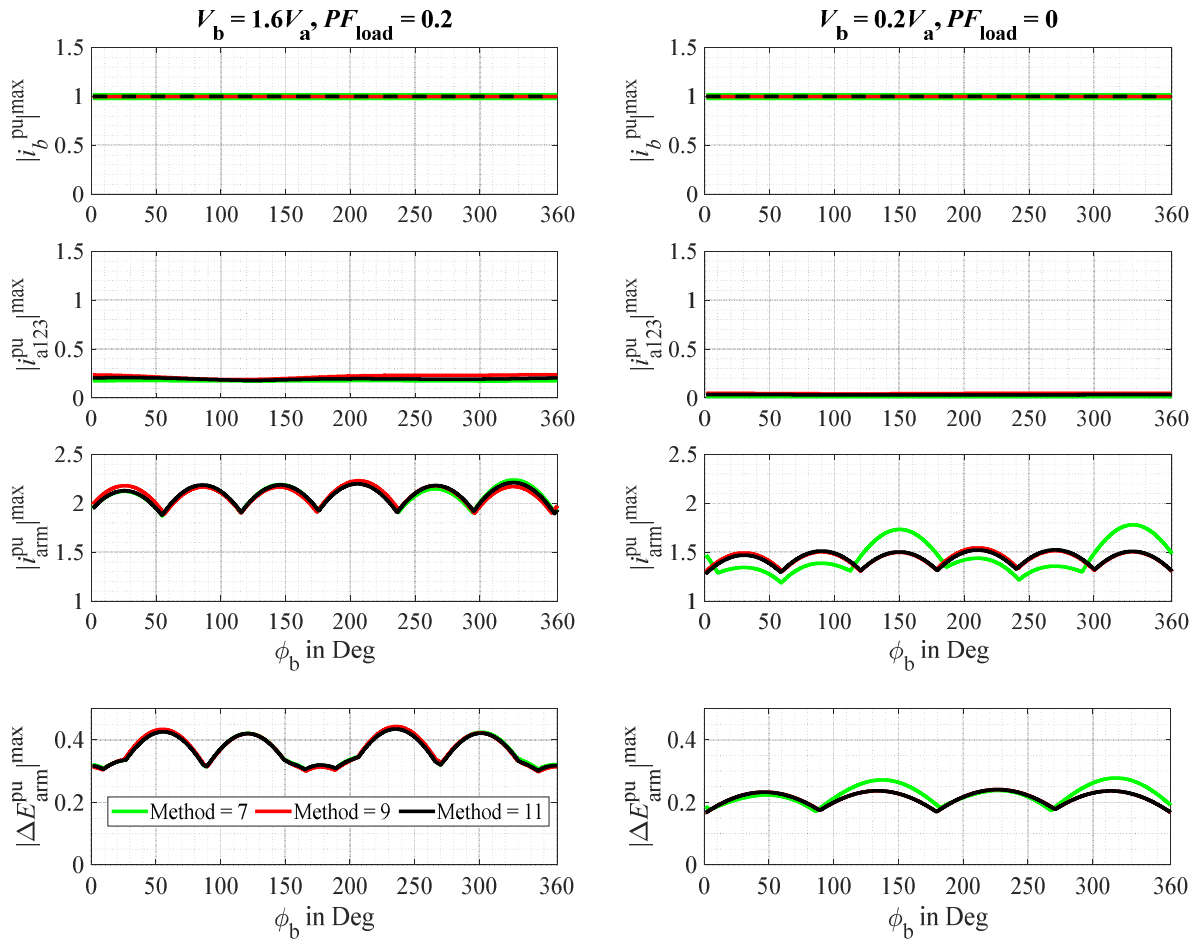

Fig. 6: Performance analysis during faulty conditions on the single-phase side of MMC for few well-behaved stable energy regulation techniques at $f_b = f_a$. Left: fault far away from MMC and Right: fault near MMC.

Conclusion

A new generalized mathematical toolchain is presented to investigate the stability and performance of all possible average arm energy regulation techniques for direct AC-AC and AC-DC MMC topologies. All proposed methods are stable for unequal frequency operations ($f_a = n f_b$, $f_b = n f_a$ & f_b = DC), where n = odd integers because the three-phase and single-phase systems are naturally decoupled. On the other hand, some methods are unstable for equal frequency operation ($f_a = f_b$) due to the coupling between the manipulated inputs. The common-mode voltage is found to be vital for the arm energy regulation techniques for equal frequency operation. For unequal frequency operation, fewer arm currents are required when the power factor of the load is small. On the other hand, more arm currents are required for equal frequency operation when the load power factor is low. Further, more ripple in the arm energies is observed with a low power factor because the reactive load power flows inside the MMC, which could not be compensated by the reactive power on the other side. The proposed toolchain can also validate the dimensioning of the direct AC-AC and AC-DC MMC topologies by analyzing the MMC energies and currents for all operating conditions of the converter (power factor, fault cases). Any existing MMC energy regulation technique could be linked directly or indirectly to all derived energy balancing methods.

In the future, it is intended to develop a similar analytical toolchain to further investigate the performance of the discussed energy balancing techniques for non-integer three-phase and single-phase frequency operation. This paper avoids this operation due to its increased complexity in computing the average mean value.

References

[1] J. Rodriguez, Jih-Sheng Lai and Fang Zheng Peng, "Multilevel inverters: a survey of topologies, controls, and applications," in IEEE Transactions on Industrial Electronics, vol. 49, no. 4, pp. 724-738, Aug. 2002, doi: 10.1109/TIE.2002.801052.

[2] L. Harnefors, S. Norrga, A. Antonopoulos and H. Nee, "Dynamic modeling of modular multilevel converters," Proceedings of the 2011 14th European Conference on Power Electronics and Applications, 2011, pp. 1-10.

[3] F. Kammerer, M. Gommeringer, J. Kolb and M. Braun, "Energy balancing of the Modular Multilevel Matrix Converter based on a new transformed arm power analysis," 2014 16th European Conference on Power Electronics and Applications, 2014, pp. 1-10, doi: 10.1109/EPE.2014.6910939.

[4] J. Kolb, F. Kammerer, M. Gommeringer and M. Braun, "Cascaded Control System of the Modular Multilevel Converter for Feeding Variable-Speed Drives," in IEEE Transactions on Power Electronics, vol. 30, no. 1, pp. 349-357, Jan. 2015, doi: 10.1109/TPEL.2014.2299894.

[5] M. Schütt and H. Eckel, "Design and analysis of complex vector current regulators for modular multilevel converters," 2017 19th European Conference on Power Electronics and Applications (EPE'17 ECCE Europe), 2017, pp. P.1-P.10, doi: 10.23919/EPE17ECCEEurope.2017.8099183.

[6] L. Angquist, A. Antonopoulos, D. Siemaszko, K. Ilves, M. Vasiladiotis and H. Nee, "Open-Loop Control of Modular Multilevel Converters Using Estimation of Stored Energy," in IEEE Transactions on Industry Applications, vol. 47, no. 6, pp. 2516-2524, Nov.-Dec. 2011, doi: 10.1109/TIA.2011.2168593.

[7] A. Antonopoulos, L. Angquist and H. Nee, "On dynamics and voltage control of the Modular Multilevel Converter," 2009 13th European Conference on Power Electronics and Applications, 2009, pp. 1-10.

[8] D. Siemaszko, A. Antonopoulos, K. Ilves, M. Vasiladiotis, L. Ängquist and H. Nee, "Evaluation of control and modulation methods for modular multilevel converters," The 2010 International Power Electronics Conference - ECCE ASIA -, 2010, pp. 746-753, doi: 10.1109/IPEC.2010.5544609.

[9] A. Lesnicar and R. Marquardt, “A new modular voltage source inverter topology,” in *Proc. 10th EPE*, Toulouse, France, 2003, pp. 1–10.

[10] A. Lesnicar and R. Marquardt, "An innovative modular multilevel converter topology suitable for a wide power range," 2003 IEEE Bologna Power Tech Conference Proceedings,, 2003, pp. 6 pp. Vol.3-, doi: 10.1109/PTC.2003.1304403.